Chemical Science

ROYAL SOCIETY OF CHEMISTRY

EDGE ARTICLE

View Article Online
View Journal | View Issue

Cite this: *Chem. Sci.*, 2022, **13**, 10375

All publication charges for this article have been paid for by the Royal Society of Chemistry

Received 20th June 2022
Accepted 8th August 2022

DOI: 10.1039/d2sc03419k

rsc.li/chemical-science

Combination of vancomycin and guanidinium-functionalized helical polymers for synergistic antibacterial activity and biofilm ablation†

Wen-Bin Liu,[b] Run-Tan Gao,[a] Li Zhou,[b] Na Liu,[a] Zheng Chen[a] and Zong-Quan Wu *[a]

The emergence of various resistant bacteria and overuse of antibiotics have led to severe side effects. Therefore, developing efficient and safe antibacterial systems is important. Herein, well-defined antimicrobial material–helical poly(phenyl guanidinium isocyanide) block copolymers with different conformations (L-P3-van, D-P3-van, and DL-P3-van) that connect vancomycin (van) to the polymer through a disulfide bond were synthesized. The prepared antimicrobial materials exhibit broad-spectrum antimicrobial activity, low bacterial resistance, and good proteolytic stability. They also overcome the intrinsic resistance of Gram-negative bacteria to van with a 100-fold increase in antimicrobial activity. Interestingly, the conformation of the material promotes its antimicrobial activity. The left-handed helix conformation shows five-fold more antimicrobial activity than the right-handed helical conformation, thereby opening a path for the application of nanochirality in the field of antibiotics.

Introduction

Recently, considerable progress has been achieved in the study of polymeric antimicrobial systems for the prevention and elimination of biofilms.[1–3] Such systems can improve biocompatibility, reduce bacterial resistance, and increase antimicrobial efficiency.[4–6] Although these polymer antimicrobial systems have been extensively examined, the effect of chirality on their antimicrobial effect remains unclear. Many biological macromolecules such as amino acids, DNA, cell-penetrating peptides, and antibacterial peptides have helical structures and are closely related to vital life functions in biological systems.[7–10] Therefore, helical biological macromolecules and their microenvironments are chiral in living systems. The chirality of the material affects physiological processes such as the body's immune response to viral infections.[11] Most effective antibiotics, such as vancomycin (van),[12] kanamycin,[13] and polymyxin B,[14] are chiral. From this perspective, the chirality of a polymer antimicrobial system may influence its antimicrobial effect. Moreover, different chiral carriers may behave differently when interacting with living systems.[15–17] A helix is a chiral expression because left- and right-handed helices cannot overlap but are mirror images of each other.[18,19] Therefore, the design and synthesis of chiral antimicrobial systems and their structure–function relationship have important significance.

The formation of biofilms in bacterial infections is a major medical challenge because biofilms can isolate bacteria from the host immune response and antibiotics. The traditional strategy to treat bacterial infections is to use antimicrobials.[20] Developed antimicrobials include antibiotics, antimicrobial peptides,[21] cationic polymers,[22,23] and other nanomaterials.[24–27] However, only a few of these materials can destroy the original biofilm.[28–30] Van is an effective antibiotic used against Gram-positive bacteria.[31] However, its overuse has led to the emergence of resistant bacteria.[32–36] Moreover, van is inherently inactive against Gram-negative bacteria because it cannot pass through the outer membrane of these bacteria.[37] Therefore, studies on Gram-positive bacteria overcoming resistance because of abuse and Gram-negative bacteria overcoming intrinsic resistance to van are warranted. Guanidine derivatives have received considerable attention for their antimicrobial potential and membrane association and penetration.[38–40] The most representative is the cell penetration peptides (CPPs), which are usually composed of short side chains and arginine-rich peptides.[41,42] These CPPs enter the cell by direct membrane penetration; alternatively, the CPPs induce membrane multilayers and then enter the cells through membrane fusion or endocytosis.[43–45]

Because of the excellent antibacterial and biofilm ablation properties of guanidine derivatives and van and the many practical problems they face, we propose a synergistic combination of guanidine polymers and van to develop an ultra-efficient antimicrobial system. Partially inspired by the cell-

[a]State Key Laboratory of Supramolecular Structure and Materials, College of Chemistry, Jilin University, Changchun 130012, China. E-mail: zqwu@jlu.edu.cn
[b]Department of Polymer Science and Engineering, Hefei University of Technology, Hefei 230009, China

† Electronic supplementary information (ESI) available. See https://doi.org/10.1039/d2sc03419k

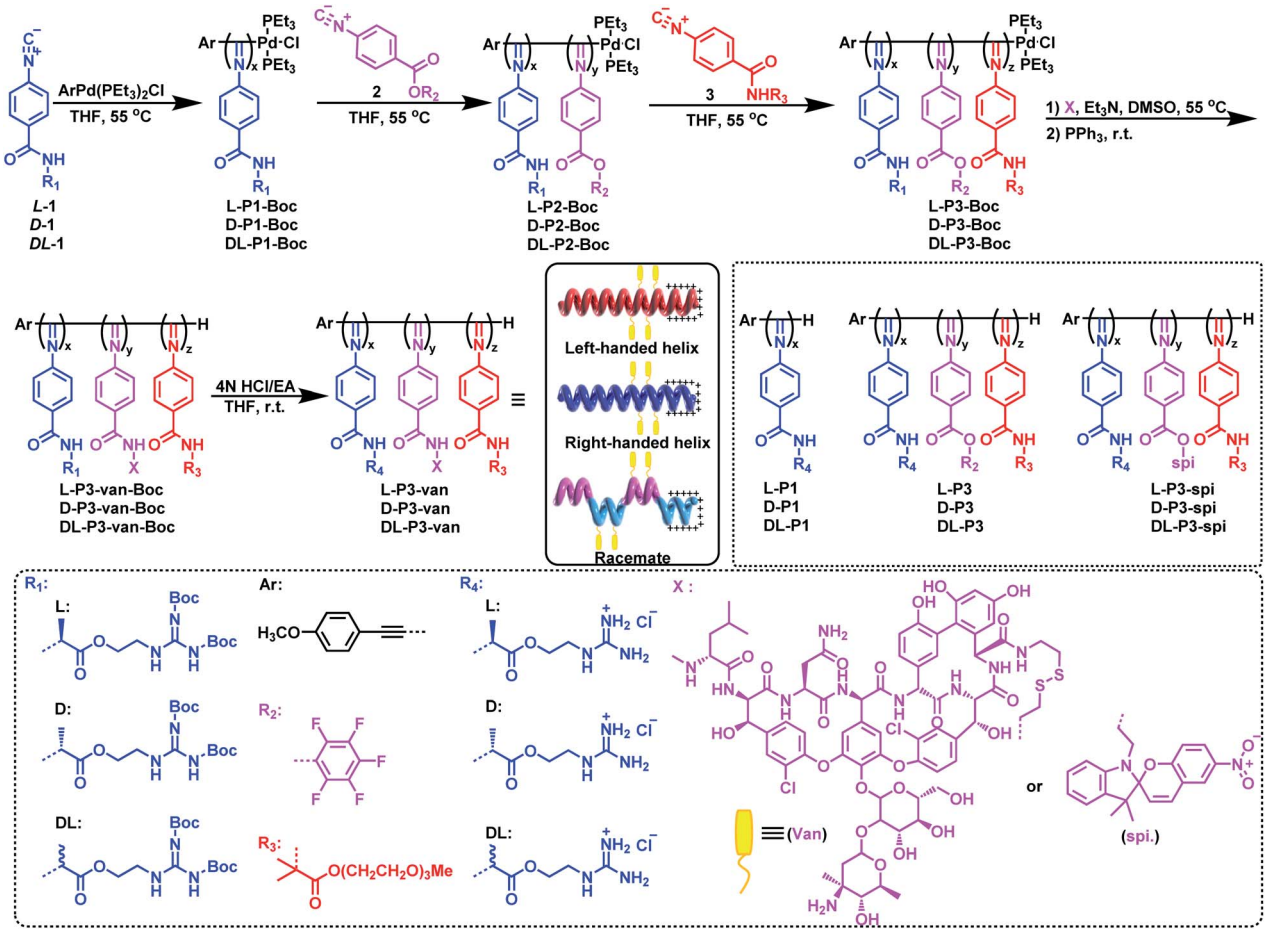

Scheme 1 Synthesis of antimicrobial nanoparticles.

penetrating peptides and biological helices, we designed and synthesized a number of helical poly(phenyl guanidinium isocyanide) block copolymers with van connected to the polymer through the disulfide bond (Scheme 1) to obtain antibacterial materials with broad-spectrum antibacterial activities, low resistance trends, good proteolytic stability, and structural flexibility.[46,47] These antimicrobial materials not only exert good antimicrobial activity against Gram-negative *Escherichia coli* and Gram-positive *Staphylococcus aureus* but also effectively disrupt the pre-formed biofilm by effectively penetrating biofilm barriers and disrupting bacteria surrounded by biofilms. The prepared antibacterial materials show up to 100-fold stronger activity against Gram-negative bacteria than van. This result can be attributed to the helical poly(phenyl guanidinium isocyanide) that can penetrate the outer membrane of Gram-negative bacteria and release van inside the bacteria for sterilization because of the cleavage of the disulfide bond by high concentrations of glutathione in the bacteria. Furthermore, the chirality of the material promotes antibacterial activity and biofilm disruption.

Results and discussion

As outlined in Scheme 1, an enantiopure phenyl isocyanide monomer L-**1** bearing L-guanidine substituent was polymerized by an alkyne-Pd(II) catalyst ($ArPd(PEt_3)_2Cl$) in THF at 55 °C ($[L\text{-}\mathbf{1}]_0/[Pd]_0 = 30$) following a living polymerization mechanism (the characterization of the monomer is shown in Fig. S1–S9 in the ESI).†[48] The resulting polymer (L-P1-Boc) demonstrated a single modal and narrow distributed elution trace on size exclusion chromatography (SEC), as shown in Fig. 1a. The number-average molecular weight (M_n) and its distribution (M_w/M_n) values were 11.7 kDa and 1.08, respectively. For chain extension of this polymer, the pentafluorophenyl ester functionalized phenyl isocyanide monomer **2** was used, and the ratio of **2**-to-Pd(II) was fixed at ~5. Based on the SEC results, when monomer **2** was completely consumed, the polymerization solution was treated with monomer **3** bearing oligoethylene glycol to afford a triblock copolymer. As shown in the SEC results in Fig. 1a, the M_n value of diblock copolymer L-P2-Boc increased to 12.1 kDa, whereas the M_w/M_n remained low (1.10). After copolymerization with monomer **3**, the elution trace of the resulting triblock copolymer L-P3-Boc shifted to a higher M_n-region while remaining unimodal and symmetric. Based on the SEC results, the M_n and M_w/M_n values of L-P3-Boc were determined to be 34.8 kDa and 1.21, respectively. The synthetic polymers were further confirmed using ^1H NMR and FT-IR analyses (Fig. S11 in the ESI†). The block ratio is 6 : 1 : 7 ($x : y : z$), which generally agrees with the proposed structure and the monomer feed ratios (Fig. S10†). In the ^{19}F NMR

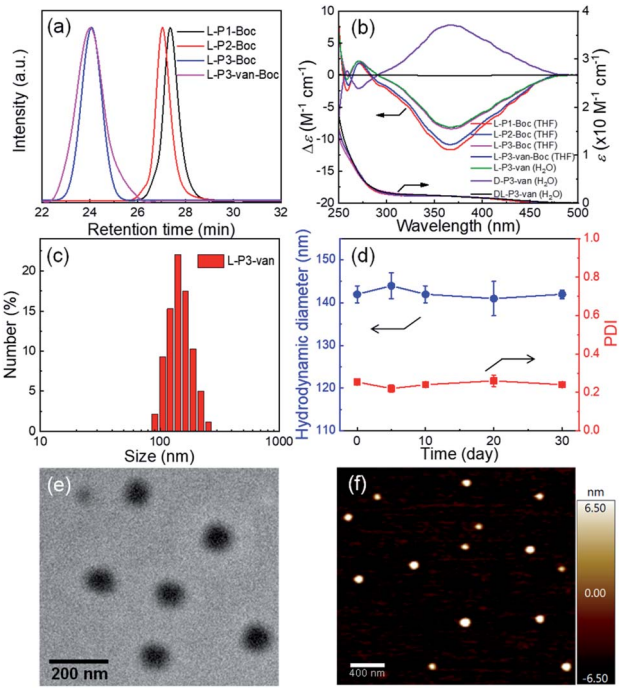

Fig. 1 (a) SEC curves of homopolymers L-P1-Boc, L-P2-Boc, L-P3-Boc and L-P3-van-Boc. (b) CD and UV-vis spectra of antibacterial nanoparticles. (c) DLS, (d) stability, (e) TEM, and (f) AFM image of L-P3-van. The error bars are based on the standard deviations of three parallel tests.

spectrum of L-P3-Boc, three broad resonances at −150, −155, and −160 ppm corresponding to the pentafluorophenol ester pendants can be clearly determined (Fig. S11†). Moreover, the characteristic vibrations of C=N and C=O bonds can be detected at 1630 and 1737 cm^{-1}, respectively, in the FT-IR spectra of the triblock copolymer L-P3-Boc, which confirmed the formation of the expected triblock copolymer (Fig. S12†).

Using the triblock copolymer, we attempted to synthesize van and guanidine synergistic antibacterial nanoparticles using van carrying the disulfide bond (van–NH_2, see the ESI† for the synthesis methods and characterization) (Scheme 1). The polymer L-P3-van-Boc was obtained by reacting van–NH_2 with the pentafluorophenol benzoate pendant of the triblock copolymer in THF using triethylamine as a catalyst. The resulting polymer was confirmed using SEC. As shown in Fig. 1a, compared with that of the precursor, the SEC trace of the polymer shifted to a shorter retention time region. Both M_n and M_w/M_n of the resulting polymer were 37.6 kDa and 1.32, respectively. In the ^1H NMR spectrum, the signals originating from van and cystamine were clearly observed (Fig. S14†). No ^{19}F resonance could be determined from the ^{19}F NMR spectra of the resulting L-P3-van-Boc (Fig. S11†). This result confirmed that almost all pentafluorophenol benzoate pendants participated in the reaction. Moreover, the characteristic vibration peaks of van were clearly visible in the FT-IR spectra of L-P3-van-Boc (Fig. S12†). Thus, the polymers carry plenty of van-units of the pendants. Subsequently, the protective Boc group was removed under acidic conditions (HCl/EA) to obtain the corresponding nano-antibacterial material L-P3-van (Scheme 1). This polymer was insoluble in organic solvents but soluble in water. The enantiomeric antipode D-P3-van and achiral DL-P3-van with similar block ratios and degree of polymerizations (DPs) of each block to those of L-P3-van were prepared using the same method (Scheme 1 and Fig. S13–S15, ESI†).

The helicity of synthetic polymers was examined using circular dichroism (CD) and UV-vis absorption spectroscopies. As shown in Fig. 1b, because of the asymmetric induction of the chiral monomer L-**1**, L-P1-Boc demonstrated intense CD at the absorption region of the poly(phenyl isocyanide) backbone, thus confirming the formation of a predominant left-handed helix. After copolymerization with achiral monomers **2** and **3**, the CD intensities decreased because of the partial helical inversion of the newly formed blocks. However, after introducing van and removing the protective Boc group, the CD was maintained as that of the triblock copolymer, suggesting that the optical activity of the helical polyisocyanide was maintained. As anticipated, D-P3-van demonstrated a mirror CD profile to that of L-P3-van, whereas DL-P3-van was CD silent (Fig. 1b). The optical activities were confirmed using the optical rotation investigation (Table 1 and Fig. S16†). The structure was stable, with almost no observable changes in CD and UV-vis spectra at the temperature range of 5 °C to 50 °C in water (Fig. S17†).

The nano-antimicrobial material L-P3-van demonstrated good solubility in water because of the presence of the guanidine group and oligoglycol chain. The hydrodynamic diameter (D_h) of L-P3-van in water determined by dynamic light scattering (DLS) was 142 nm (Fig. 1c). A prolonged standing study demonstrated that the D_h and polydispersity index remained almost unchanged over a month (Fig. 1d). Accordingly, the D_hs values of DL-P3-van and D-P3-van were 137 and 136 nm, respectively (Fig. S18a and d†). The morphology of L-P3-van was investigated by transmission electron microscopy (TEM) and atomic force microscopy (AFM). As shown in Fig. 1e and f, L-P3-van demonstrated spherical nanoparticles in the TEM and AFM images. The average diameters of these nanoparticles were estimated to be 110 and 115 nm, as determined by TEM and AFM, respectively; generally, these results agree with the DLS analyses. Accordingly, both TEM and AFM studies demonstrated that DL-P3-van and D-P3-van had similar spherical morphologies and sizes to those of L-P3-van due to the similar block ratios and DPs of the three polymers (Fig. S18, ESI†). The driving force for self-assembly is not very clear at the current stage, while the different solvophobic effects of the three blocks in water may have great contribution to the assembly.[10] The self-assembled micelles have locally enriched positive charges, and thus favor enhanced antimicrobial activity and selectivity.[49]

Then, the antibacterial potential of the three polymers was evaluated against Gram-positive *S. aureus* (ATCC25923) and Gram-negative *E. coli* (O157), and the results are summarized in Tables 1 and S2 and Fig. S19 in the ESI.† The minimum inhibitory concentration (MIC) is defined as the lowest polymer concentration required to inhibit 100% bacterial growth after an incubation period of 18 h.[50] For Gram-positive *S. aureus*, van demonstrated potent antimicrobial activity against extracellular

Table 1 The characterization data for the polymers

Samples[a]	Size[b] (nm)	ε_{364}[c] (M^{-1} cm^{-1})	MIC (μM)		MBEC (μM)		HC_{50} (μM)	Selectivity HC_{50}/MIC_{90}	
			[d]*E. coli*	[e]*S. aureus*	*E. coli*	*S. aureus*	[f]RBC	*E. coli*	*S. aureus*
DL-P3-Van	137	—	1.5	0.8	45	4	150	10	187.5
L-P3-Van	142	−8.10	0.5	0.2	15	1	150	30	750
D-P3-Van	136	+7.80	2	1	70	5	150	7.5	150

[a] The polymers were synthesized according to ESI Scheme S2. [b] Determined by dynamic light scattering. [c] Measured in water at 25 °C (c = 0.2 mg mL^{-1}). [d] *E. coli* (O157). [e] *S. aureus* (ATCC25923). [f] Rat red blood cells.

S. aureus (MIC = 0.69 μM), which was consistent with the literature.[51] Compared with the antibacterial activity of van, the antimicrobial activity of the synthetic polymers increased by ~30–100 fold after the introduction of van. Interestingly, the helicity of polymers resulted in different antimicrobial effects, although they have similar DPs and block ratios. Compared with the antibacterial activities of DL-P3-van and D-P3-van with MIC = 0.8 and 1 μM, respectively, L-P3-van had a stronger antibacterial activity (MIC = 0.2 μM). This result can be attributed to the left-handed antibacterial polymer acting on the cell membrane faster than the antimicrobial materials with racemic and right-handed helices. As shown in Fig. 2a, the bactericidal efficiency of L-P3-van at ~2 μM was >99%, and its antibacterial activity was comparable to that of van. Similarly, the antimicrobial activity of L-P3-van against *E. coli* was ~15–40 fold higher than that of van alone. Even at higher concentrations, van does not naturally have high antibacterial activity (MIC = 50 μM) against Gram-negative bacteria. When it was introduced in the helical polymer, its antibacterial activity increased by up to 100-fold. Note that the bactericidal efficiency of L-P3-van at 5 μM exceeded 99% for *E. coli* (Fig. 2b). A series of copolymers with different block ratios of van to guanidinium and oligoglycol segments were prepared and evaluated against two typical bacteria, *E. coli* and *S. aureus* (Fig. S20–S24, ESI†). For both *S. aureus* and *E. coli*, the introduction of van and the guanidine groups into the copolymers was beneficial for increasing the antimicrobial activity, while the ratios of van to guanidinium and to oligoglycol moieties have a slight influence on the antibacterial properties.

The hemolytic concentration-50% (HC_{50}) of polymers was determined against freshly drawn mouse red blood cells (RBCs) to assess the toxicity toward mammalian cells.[52] HC_{50} is defined as the lowest polymer concentration required to lyse 50% of the RBCs within an incubation period of 1 h. The highest concentration of polymer solution tested was 2000 μg mL^{-1}.[50] As summarized in Table S2,† homopolymers DL-P1, L-P1, and D-P1 were highly antibacterial against *E. coli* and *S. aureus* but extremely hemolytic (HC_{50} = 1.3 μM). After introducing the oligoglycol segment, the hemolytic activity of the material decreased, and the HC_{50} values corresponding to DL-P3, L-P3, and D-P3 were 135 μM. This result can be attributed to the oligoglycol segments resisting protein adsorption, providing stealth properties, modifying the hydrophilic/hydrophobic balance of the polymer structure, and reducing the electrostatic repulsion between the amphipathic polymer chains.[53–56] Although the oligoglycol pendants are short, the polymeric backbone bearing plenty of oligoglycol pendants could resist protein adsorption.[54–56] For comparison, owing to protein adsorption, L-P2 without oligoglycol pendants was precipitated when treated with *S. aureus* (Fig. S25, ESI†).

Bacteria with and without the presence of antibiotic polymers were cultured in Petri dishes to evaluate their antibiotic effects. As shown in Fig. 2c, DL-P3-van, L-P3-van, and D-P3-van demonstrated high sterilization effects on *E. coli* and *S. aureus*, of which the left-handed L-P3-van demonstrated the best performance. Fluorescence microscopy imaging experiments were performed to visualize the viable and inactive bacteria.

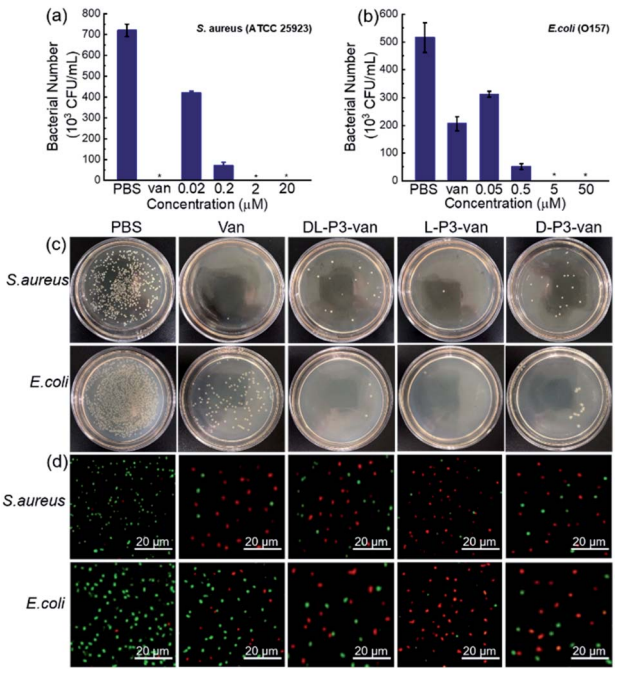

Fig. 2 Antibacterial ability of L-P3-van against (a) *S. aureus*, (b) *E. coli* and van (2 and 25 μM) as the positive controls, respectively. PBS as the negative control. * indicates no detection of bacteria in the plate counting experiments. The error bars indicate the standard deviations of triplicate experiments. (c) Photographs obtained by culturing the sample solutions from *S. aureus* and *E. coli* incubated with PBS, DL-P3-van, L-P3-van and D-P3-van solution on individual Petri dishes and (d) corresponding fluorescence microscopic images of *S. aureus* and *E. coli* that were stained with calcein-AM/PI dyes.

Calcein-AM was used to label the viable cells with green fluorescence, whereas PI with red fluorescence merely penetrated bacteria with damaged cell membranes. As shown in Fig. 2d, nearly all *S. aureus* and *E. coli* cells were stained red with PI after the L-P3-van treatment, indicating the disintegration of bacterial membranes. However, very rare red fluorescence was observed in the phosphate-buffered saline (PBS) group. The bacteria exhibited green and red fluorescence for the other formulations of van, DL-P3-van, and D-P3-van, suggesting an incomplete bacterial killing. These results demonstrated that the antimicrobial polymers killed the bacteria by destroying their membranes and cell walls. In addition to the disruptive interactions of the guanidine group with the cell membrane, the ability of van to block the cell wall growth contributes to the increased antimicrobial capacity.[57,58]

The SEM observations revealed that the bacteria treated with L-P3-van, D-P3-van, and DL-P3-van were ruptured, and the morphology hardly maintained integrity, especially that of the L-P3-van-treated bacteria (Fig. 3b–d and f–h). The PBS-treated bacteria had complete morphology and a smooth surface (Fig. 3a and e). Then, the protein leakage from the bacteria was first explored using the Bradford protein assay kit. All treatments of van, DL-P3-van, L-P3-van, and D-P3-van resulted in a certain amount of protein leakage, indicating that the membrane was damaged to a certain extent (Fig. S26†). As expected, the L-P3-van-treated bacteria displayed the largest amount of protein leakage and the maximum membrane damage, which is consistent with the SEM observations.

To investigate the effect of the helical conformation on the antibacterial effects of the antimicrobial materials, we introduced the fluorescein spiropyran (spi.) into the helical polymers to synthesize three fluorescent markers with different conformations (L-P3-spi, D-P3-spi, and DL-P3-spi, see the ESI† for the synthesis methods and characterization Fig. S27 and S28†). Because of the fluorescence properties of the polymer itself, antibacterial processes were monitored for different materials by confocal microscopy. As shown in Fig. 4, *S. aureus* was detreated with L-P3-spi, D-P3-spi, and DL-P3-spi. After 1 h, visible fluorescence was observed in the bacteria treated with L-P3-spi under confocal microscopy but not in the bacteria treated with D-P3-spi and DL-P3-spi after ~5 h (Fig. S29, ESI†). After 7 h, a large area of *S. aureus* was observed by confocal microscopy and labeled by using the left-handed L-P3-spi. This result suggests that the left-handed polymer acted faster on the bacterial cell membranes than the other two polymers. These antimicrobial polymers carrying van and guanidinium pendants kill the bacteria by destroying their membrane and cell walls. Thus, the polymer acting faster on the bacteria can kill the bacteria more quickly and showed better antibacterial properties.[11,59] The L-P3-van, D-P3-van, and DL-P3-van polymers have similar DPs and block ratios, and are self-assembled into micelles of similar sizes in water. The different antibacterial properties of these polymers were probably ascribed to the different chirality and handedness of the backbone, which resulted in left- and right-handed packing of the van and guanidinium pendants on L-P3-van and D-P3-van, respectively, while the van and guanidinium pendants of DL-P3-van may packed in a random way. The different arrays of the pendants thus resulted in different antibacterial properties.

Encouraged by the performance of DL-P3-van, L-P3-van, and D-P3-van against bacterial cells, we evaluated the efficacy of DL-P3-van, L-P3-van, and D-P3-van as agents to disrupt bacterial biofilms. *S. aureus* and *E. coli* biofilms were pre-cultivated and then treated with DL-P3-van, L-P3-van, and D-P3-van for another 24 h. The resulting bacterial growth in biofilms was observed by measuring the optical density at 600 nm (OD_{600}). PBS as a negative control and van as a positive control were employed. Crystal-violet staining and the minimum biofilm eradication

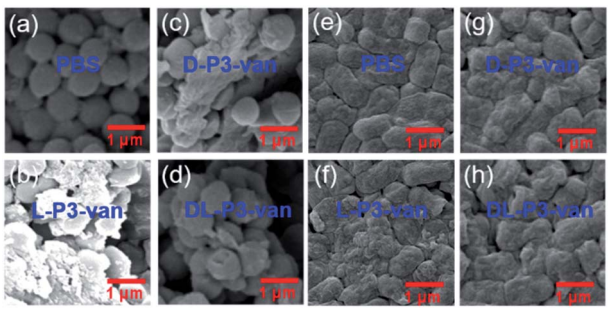

Fig. 3 SEM images of (a)–(d) *S. aureus* and (e)–(h) *E. coli* treated with PBS, L-P3-van, D-P3-van and DL-P3-van.

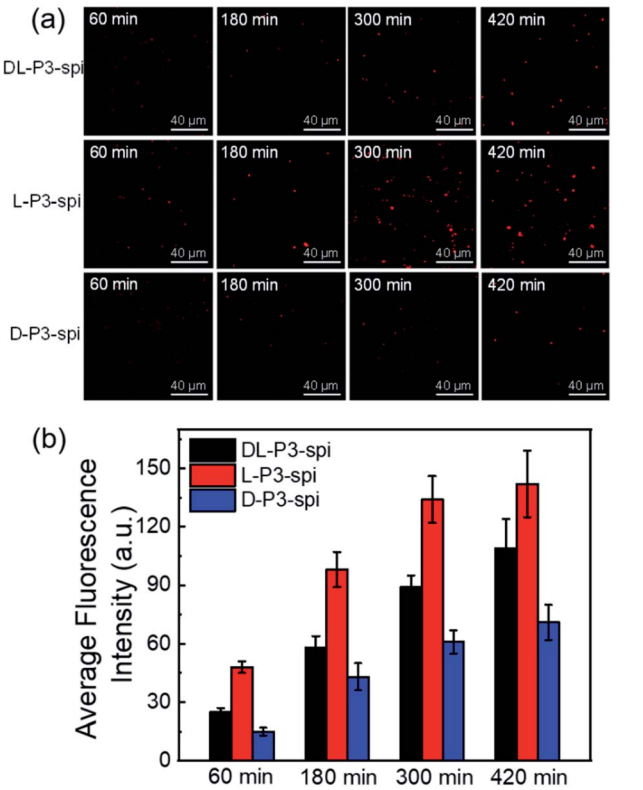

Fig. 4 (a) Real-time monitoring of DL-P3-spi, L-P3-spi and D-P3-spi infecting *S. aureus*. (b) Fluorescence intensities per image for bacteria treated with DL-P3-spi, L-P3-spi and D-P3-spi, as calculated by ImageJ software.

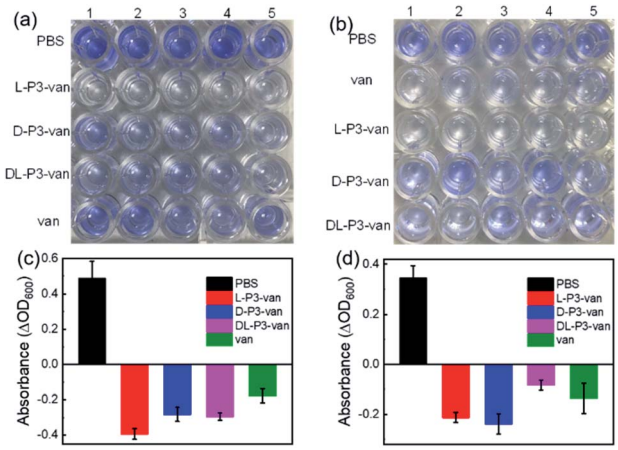

Fig. 5 Inhibition of (a) *E. coli* and (b) *S. aureus* biofilm formation by different antimicrobial materials stained with crystal violet. Each concentration of compound was tested in five wells. (c) *E. coli* and (d) *S. aureus* growth after treatment with different antimicrobial materials for 1 day in biofilm stages.

concentration assay were performed to accurately evaluate the biofilm inhibition and eradication activities of DL-P3-van, L-P3-van, and D-P3-van (Fig. 5, S30 and S31 in the ESI†).

As summarized in Tables 1 and S2,† biofilm inhibition and eradication effects could be observed at 5 μM, which indicated that DL-P3-van, L-P3-van, and D-P3-van have potential to be therapeutic agents to tackle biofilm-associated infections. Although the actual mechanism of biofilm disruption is under investigation, we believe the following factors play major roles. First, the positively charged polymers could perturb the negatively charged exopolysaccharide matrix of biofilms through electrostatic and hydrophobic interactions.[38–40] Second, these helical polymers can act as cell-penetrating peptides to cross the membrane into the cell interior,[9,60,61] releasing van and thus hindering the synthesis of the bacterial cell wall, ultimately leading to biofilm degradation.[59]

Conclusions

We designed and synthesized a series of well-defined helical polymers (L-P3-van, D-P3-van, and DL-P3-van) with a redox stimulus-responsive release of van for preparing synergistic antibacterial and ablation biofilms. These antimicrobial materials demonstrated broad-spectrum antibacterial activities, low bacterial resistance, and good proteolytic stability. L-P3-Van exhibited high activity, which was 100-fold higher than that achieved by van. This result can be attributed to the fact that helical poly(phenyl guanidinium isocyanide) can penetrate the outer membrane of Gram-negative bacteria, thus releasing van into the Gram-negative bacteria for sterilization. Interestingly, the chirality of the material promoted the antibacterial activity and disruption of biofilms. Both antimicrobial and confocal microscopic experiments demonstrated that the material with a left-handed helical conformation performed better with respect to antibacterial activity and biofilm removal. To summarize, these results reveal that the prepared helical polymers are efficient and safe antibacterial systems with essential application prospects for treating bacterial infections and ablating biofilms *in vivo*.

Data availability

The detailed experimental data associated with this work are available in the ESI.†

Author contributions

W.-B. L., R.-T. G. and L. Z. performed the experiments and analyses. W.-B. L. and Z.-Q. W. wrote and edited the paper. N. L., Z. C. and Z.-Q. W. conceived the idea and supervised the research.

Conflicts of interest

There are no conflicts to declare.

Acknowledgements

We acknowledge the National Natural Science Foundation of China for financial support (NSFC, No. 22071041, 21971052, 51903072, and 21871073). L. Zhou and Z.-Q. Wu appreciate the Fundamental Research Funds for the Central Universities of China (Grant No. PA2019GDPK0057, and PA2020GDJQ0028).

Notes and references

1 S. Eckhardt, P. S. Brunetto, J. Gagnon, M. Priebe, B. Giese and K. M. Fromm, *Chem. Rev.*, 2013, **113**, 4708–4754.
2 A. Gupta, S. Mumtaz, C.-H. Li, I. Hussain and V. M. Rotello, *Chem. Soc. Rev.*, 2019, **48**, 415–427.
3 M. Krishnamoorthy, S. Hakobyan, M. Ramstedt and J. E. Gautrot, *Chem. Rev.*, 2014, **114**, 10976–11026.
4 L. Gao, M. Li, S. Ehrmann, Z. Tu and R. Haag, *Angew. Chem., Int. Ed.*, 2019, **58**, 3645–3649.
5 S. Guo, Q. Huang, Y. Chen, J. Wei, J. Zheng, L. Wang, Y. Wang and R. Wang, *Angew. Chem., Int. Ed.*, 2021, **60**, 618–623.
6 A. Antonoplis, X. Zang, M. A. Huttner, K. K. L. Chong, Y. B. Lee, J. Y. Co, M. R. Amieva, K. A. Kline, P. A. Wender and L. Cegelski, *J. Am. Chem. Soc.*, 2018, **140**, 16140–16151.
7 J. D. Watson and F. H. C. Crick, *Nature*, 1953, **171**, 737–738.
8 B. T. Stokke, A. Elgsaeter, D. A. Brant and S. Kitamura, *Macromolecules*, 1991, **24**, 6349–6351.
9 Z. Li, D. Teng, R. Mao, X. Wang, Y. Hao, X. Wang and J. Wang, *J. Med. Chem.*, 2018, **61**, 7991–8000.
10 M. Xiong, M. W. Lee, R. A. Mansbach, Z. Song, Y. Bao, R. M. Peek Jr., C. Yao, L.-F. Chen, A. L. Ferguson, G. C. L. Wong and J. Cheng, *PNAS*, 2015, **112**, 13155–13160.
11 L. Xu, X. Wang, W. Wang, M. Sun, W. J. Choi, J.-Y. Kim, C. Hao, S. Li, A. Qu, M. Lu, X. Wu, F. M. Colombari, W. R. Gomes, A. L. Blanco, A. F. de Moura, X. Guo, H. Kuang, N. A. Kotov and C. Xu, *Nature*, 2022, **601**, 366–373.

12 F. Umsttter, C. Domhan, T. Hertlein, K. Ohlsen, E. Mühlberg, C. Kleist, S. Zimmermann, B. Beijer, K. D. Klika, U. Haberkorn, W. Mier and P. Uhl, *Angew. Chem., Int. Ed.*, 2020, **59**, 8823–8827.
13 A. Brezden, M. F. Mohamed, M. Nepal, J. S. Harwood, J. Kuriakose, M. N. Seleem and J. Chmielewski, *J. Am. Chem. Soc.*, 2016, **138**, 10945–10949.
14 A. Luther, M. Urfer, M. Zahn, M. Müller, S.-Y. Wang, M. Mondal, A. Vitale, J.-B. Hartmann, T. Sharpe, F. Lo Monte, H. Kocherla, E. Cline, G. Pessi, P. Rath, S. M. Modaresi, P. Chiquet, S. Stiegeler, C. Verbree, T. Remus, M. Schmitt, C. Kolopp, M.-A. Westwood, N. Desjonquères, E. Brabet, S. Hell, K. LePoupon, A. Vermeulen, R. Jaisson, V. Rithié, G. Upert, A. Lederer, P. Zbinden, A. Wach, K. Moehle, K. Zerbe, H. H. Locher, F. Bernardini, G. E. Dale, L. Eberl, B. Wollscheid, S. Hiller, J. A. Robinson and D. Obrecht, *Nature*, 2019, **576**, 452–458.
15 Y. Bao, Y. Huang, M. L. Lam, T. Xu, N. Zhu, Z. Guo, X. Cui, R. H. W. Lam and T. Chen, *ACS Appl. Mater. Interfaces*, 2016, **8**, 17976–17986.
16 X. Wang, C. Yan, K. Ye, Y. He, Z. Li and J. Ding, *Biomaterials*, 2013, **34**, 2865–2874.
17 W. Liu, Y. Bao, M. L. Lam, T. Xu, K. Xie, H. S. Man, E. Y. Chan, N. Zhu, R. H. W. Lam and T. Chen, *ACS Nano*, 2016, **10**, 7409–7417.
18 H. Huang, J. Deng and Y. Shi, *Macromolecules*, 2016, **49**, 2948–2956.
19 C. Tsiamantas, X. de Hatten, C. Douat, B. Kauffmann, V. Maurizot, H. Ihara, M. Takafuji, N. Metzler-Nolte and I. Huc, *Angew. Chem., Int. Ed.*, 2016, **55**, 6848–6852.
20 K. Bush, P. Courvalin, G. Dantas, J. Davies, B. Eisenstein, P. Huovinen, G. A. Jacoby, R. Kishony, B. N. Kreiswirth, E. Kutter, S. A. Lerner, S. Levy, K. Lewis, O. Lomovskaya, J. H. Miller, S. Mobashery, L. J. V. Piddock, S. Projan, C. M. Thomas, A. Tomasz, P. M. Tulkens, T. R. Walsh, J. D. Watson, J. Witkowski, W. Witte, G. Wright, P. Yeh and H. I. Zgurskaya, *Nat. Rev. Microbiol.*, 2011, **9**, 894–896.
21 M. Zasloff, *Nature*, 2002, **415**, 389–395.
22 G. N. Tew, R. W. Scott, M. L. Klein and W. F. DeGrado, *Acc. Chem. Res.*, 2010, **43**, 30–39.
23 K. Fukushima, J. P. K. Tan, P. A. Korevaar, Y. Y. Yang, J. Pitera, A. Nelson, H. Maune, D. J. Coady, J. E. Frommer, A. C. Engler, Y. Huang, K. Xu, Z. Ji, Y. Qiao, W. Fan, L. Li, N. Wiradharma, E. W. Meijer and J. L. Hedrick, *ACS Nano*, 2012, **6**, 9191–9199.
24 J. T. Seil and T. J. Webster, *Int. J. Nanomed.*, 2012, **7**, 2767–2781.
25 K. Liu, Y. Liu, Y. Yao, H. Yuan, S. Wang, Z. Wang and X. Zhang, *Angew. Chem. Int. Ed.*, 2013, **52**, 8285–8289; *Angew. Chem.*, 2013, **125**, 8443–8447.
26 I. Roy, D. Shetty, R. Hota, K. Baek, J. Kim, C. Kim, S. Kappert and K. Kim, *Angew. Chem. Int. Ed.*, 2015, **54**, 15152–15155; *Angew. Chem.*, 2015, **127**, 15367–15370.
27 L.-S. Wang, A. Gupta and V. M. Rotello, *ACS Infect. Dis.*, 2016, **2**, 3–4.
28 S. I. Maffioli, in *Antibiotics*, ed. C. O. Gualerzi, L. Brandi, A. Fabbretti and C. L. Pon, Wiley-VCH, Weinheim, 2013, pp. 1–22.
29 K. Dua, S. D. Shukla, R. K. Tekade and P. M. Hansbro, *Drug Delivery Transl. Res.*, 2017, **7**, 179–187.
30 Y. Liu, H. J. Busscher, B. Zhao, Y. Li, Z. Zhang, H. C. van der Mei, Y. Ren and L. Shi, *ACS Nano*, 2016, **10**, 4779–4789.
31 H.-Z. Lai, W.-Y. Chen, C.-Y. Wu and Y.-C. Chen, *ACS Appl. Mater. Interfaces*, 2015, **7**, 2046–2054.
32 F. von Nussbaum, M. Brands, B. Hinzen, S. Weigand and D. Häbich, *Angew. Chem., Int. Ed.*, 2006, **45**, 5072–5129.
33 T. M. Coque, J. F. Tomayko, S. C. Ricke, P. C. Okhyusen and B. E. Murray, *Antimicrob. Agents Chemother.*, 1996, **40**, 2605–2609.
34 World Health Organization, *Antimicrobial Resistance: Global Report on Surveillance, 2014*, **https://www.who.int/drugresistance/documents/surveillancereport/en/>**, 2014, accessed 1–10–17.
35 R. R. Watkins and R. A. Bonomo, *Infect. Dis. Clin. North Am.*, 2016, **30**, 313–322.
36 K. E. Jones, N. G. Patel, M. A. Levy, A. Storeygard, D. Balk, J. L. Gittleman and P. Daszak, *Nature*, 2008, **451**, 990–993.
37 V. Yarlagadda, G. B. Manjunath, P. Sarkar, P. Akkapeddi, K. Paramanandham, B. R. Shome, R. Ravikumar and J. Haldar, *ACS Infect. Dis.*, 2016, **2**, 132–139.
38 A. Antonoplis, X. Zang, M. A. Huttner, K. K. L. Chong, Y. B. Lee, J. Y. Co, M. R. Amieva, K. A. Kline, P. A. Wender and L. Cegelski, *J. Am. Chem. Soc.*, 2018, **140**, 16140–16151.
39 T. Böttcher, I. Kolodkin-Gal, R. Kolter, R. Losick and J. Clardy, *J. Am. Chem. Soc.*, 2013, **135**, 2927–2930.
40 E. G. Stanzl, B. M. Trantow, J. R. Vargas and P. A. Wender, *Acc. Chem. Res.*, 2013, **46**, 2944–2954.
41 E. Lei, M. P. Pereira and S. O. Kelley, *Angew. Chem., Int. Ed.*, 2013, **52**, 9660–9663.
42 A. Brezden, M. F. Mohamed, M. Nepal, J. S. Harwood, J. Kuriakose, M. N. Seleem and J. Chmielewski, *J. Am. Chem. Soc.*, 2016, **138**, 10945–10949.
43 W. B. Kauffman, T. Fuselier, J. He and W. C. Wimley, *Trends Biochem. Sci.*, 2015, **40**, 749–764.
44 C. Allolio, A. Magarkar, P. Jurkiewicz, K. Baxova, M. Javanainen, P. E. Mason, R. Sachl, M. Cebecauer, M. Hof, D. Horinek, V. Heinz, R. Rachel, C. M. Ziegler, A. Schrofel and P. Jungwirth, *Proc. Natl. Acad. Sci. U. S. A.*, 2018, **115**, 11923–11928.
45 F. Sgolastra, B. M. Deronde, J. M. Sarapas, A. Som and G. N. Tew, *Acc. Chem. Res.*, 2013, **46**, 2977–2987.
46 D. I. Andersson, D. Hughes and J. Z. Kubicek-Sutherland, *Drug Resistance Updates*, 2016, **26**, 43–57.
47 M. Mahlapuu, J. Håkansson, L. Ringstad and C. Björn, *Front. Cell. Infect. Microbiol.*, 2016, **6**, 194.
48 Y.-X. Xue, J.-L. Chen, Z.-Q. Jiang, Z.-P. Yu, N. Liu, J. Yin, Y.-Y. Zhu and Z.-Q. Wu, *Polym. Chem.*, 2014, **5**, 6435–6438.
49 H. Sun, Y. Hong, Y. Xi, Y. Zou, J. Gao and J. Du, *Biomacromolecules*, 2018, **19**, 1701–1720.
50 A. Punia, A. Mancuso, P. Banerjee and N.-L. Yang, *ACS Macro Lett.*, 2015, **4**, 426–430.

51 R. O. Darouiche and R. J. Hamill, *Antimicrob. Agents Chemother.*, 1994, **38**, 1059–1064.
52 P. Sahariah, B. E. Benediktssdottir, M. A. Hjalmarsdottir, O. E. Sigurjonsson, K. K. Sorensen, M. B. Thygesen, K. J. Jensen and M. Masson, *Biomacromolecules*, 2015, **16**, 1449–1460.
53 S. Zhao, W. Huang, C. Wang, Y. Wang, Y. Zhang, Z. Ye, J. Zhang, L. Deng and A. Dong, *Biomacromolecules*, 2020, **21**, 5269–5281.
54 T.-K. Nguyen, S. Lam, K. K. K. Ho, N. Kumar, G. G. Qiao, S. Egan, C. Boyer and E. H. H. Wong, *ACS Infect. Dis.*, 2017, **3**, 237–248.
55 B. Zhang, M. Li, M. Lin, X. Yang and J. Sun, *Biomater. Sci.*, 2020, **8**, 6969–6977.
56 M. Krishnamoorthy, S. Hakobyan, M. Ramstedt and J. E. Gautrot, *Chem. Rev.*, 2014, **114**, 10976–11026.
57 C. Watanakunakorn, *Clin. Infect. Dis.*, 1981, **3**, S210–S215.
58 N. E. Allen, J. N. Hobbes and T. I. Nicas, *Antimicrob. Agents Chemother.*, 1996, **40**, 2356–2362.
59 Y.-F. Zhang, X.-P. Hou, G. Wu, R.-C. Li, X.-W. Qiao, H. T. Tien and A. Ottova, *Electrochem. Commun.*, 1999, **1**, 238–241.
60 J. M. Hyman, E. I. Geihe, B. M. Trantow, B. Parvin and P. A. Wender, *PNAS*, 2012, **109**, 13225–13230.
61 J. B. Rothbard, T. C. Jessop, R. S. Lewis, B. A. Murray and P. A. Wender, *J. Am. Chem. Soc.*, 2004, **126**, 9506–9507.